The International Journal of Advanced Manufacturing Technology (2023) 124:2299–2312
https://doi.org/10.1007/s00170-022-10605-5

ORIGINAL ARTICLE

Theoretical and experimental research of edge inclination angle effect on minimum uncut chip thickness in oblique cutting of C45 steel

Tadeusz Mikołajczyk[1] · Hubert Latos[1] · Zygmunt Szczepaniak[1] · Tomasz Paczkowski[1] · Danil Yu. Pimenov[2] · Khaled Giasin[3] · Mustafa Kuntoğlu[4]

Received: 30 July 2022 / Accepted: 24 November 2022 / Published online: 11 December 2022

Abstract

The minimum uncut chip thickness (MUCT) is an important phenomenon observed both in orthogonal and oblique cutting. Rounding the cutting edge influences the initiation of the cutting process and chip formation. In a previous study, the authors presented a theoretical analysis and experimental validation on the effect of edge inclination angle λ_s in the range of 0° to 60° on $h_{\min}$ in radial-free turning of C45 steel. The current work investigated the MUCT $h_{\min}$ in oblique cutting process of C45 steel, for extremely high value of edge inclination angle λ_s. In this research, a special technique based on milling tool machine using a special tool and sample is presented. Enabled model tests in the unprecedented range of angles λ_s not used in research to date. The samples were machined using a cutting speed $v_c = 0.063$ m/min. Vertical feed of edge f_v was determined by association on the applied sample slope ($\tau = 0.60$–0.85 mm/m) and cutting speed v_c. as $f_v = 37.8$—53.5 µm/min. MUCT $h_{\min}$ parameter was measured using compensation for the effects of deformation, based on profilogram analysis. The machining experiments were carried out using a tool with $r_n = 185$ µm. It was found that in the range of angles of $50° \le \lambda_s \le 85°$, the MUCT decreases from $h_{\min} = 12$ µm for $\lambda_s = 50°$ to $h_{\min} = 4$ µm for $\lambda_s = 85°$. Increasing λ_s by 35° resulted in up to threefold reduction in MUCT. The analysis of the experimental results of $h_{\min}$ for the range of studied λ_s angle confirmed authors previously reported theory for extreme values of λ_s. In optimization procedure based on LSM, chip flow angle coefficient was determined as $k = 0.75$ and critical value of rake angle $\gamma_{cf} = -64.8°$. This feature provides prediction of results with great accuracy to experimental value. The findings from this study opens the possibility of developing new tools for finishing operations in the field of oblique cutting with high values of λ_s angle. In addition, the results introduce new area for research on improving the surface quality based on lowering the effect of MUCT on surface roughness and explaining some aspects related to surface wear in the friction process.

Keywords Oblique cutting · Machining · Minimum uncut chip thickness · Edge inclination angle

Nomenclature

MUCT	Minimum uncut chip thickness
LSM	Least square method
Oxyz	Orthogonal system of tool geometry dimension
Olmn	Oblique system of tool geometry dimension
P_r	Main plane

✉ Tadeusz Mikołajczyk
tami@pbs.edu.pl

✉ Hubert Latos
hubert.latos@utp.edu.pl

✉ Zygmunt Szczepaniak
zs@pro.onet.pl

✉ Tomasz Paczkowski
tompacz@pbs.edu.pl

✉ Danil Yu. Pimenov
danil_u@rambler.ru

✉ Khaled Giasin
Khaled.giasin@port.ac.uk

✉ Mustafa Kuntoğlu
mkuntoglu@selcuk.edu.tr

[1] Department of Production Engineering, Bydgoszcz University of Science and Technology, Al. Prof. S. Kaliskiego 7, 85-796 Bydgoszcz, Poland

[2] Department of Automated Mechanical Engineering, South Ural State University, Lenin Prosp. 76, Chelyabinsk 454080, Russia

[3] School of Mechanical and Design Engineering, University of Portsmouth, Portsmouth PO1 3DJ, UK

[4] Mechanical Engineering Department, Selcuk University, Technology Faculty, Konya 42130, Turkey

P_n	Normal section plane
P_o	Main section plane
P_f	Feed section plane
P_s	Plane of cutting
P_{cf}	Chip flow section plane
λ_s	Edge inclination angle (°)
κ_{rN}	Major cutting edge angle (°)
γ_f, γ_{fi}	Rake angle in feed direction (°)
γ_o, γ_{oi}	Main rake angle (°)
γ_n, γ_{ni}	Normal rake angle (°)
γ_{cf}, γ_{cfi}	Rake angle in the chip flow direction (°)
η_{cf}	Angle of chip flow direction (°)
k	Coefficient for η_{cf} calculation
α_o	Clear angle (°)
α_n	Normal clear angle (°)
β	Edge angle (°)
v	Direction of cutting speed
v_c	Cutting speed (m/min)
f	Feed of mill machine tool (mm/min)
f_v	Feed vertical (μm/min)
a_p	Depth of cut (mm)
c_i	Thickness of machining layer (μm)
h_r	Actual (real) uncut chip thickness (μm)
h	Nominal uncut chip thickness (μm)
$h_{\min}$	Minimum uncut chip thickness (μm)
r_n	Radius of the cutting edge rounding (μm)
r_e	Radius of circle strictly tangent to the top of the ellipse (μm)
η	Direction chip flow
ρ	Radius of ellipse
A	Half-ax of ellipse
B	Axle of the ellipse
x_o, y_o	Points on the ellipse
w	Width of sample (mm)
l	Length of cutting edge (mm)
m_T	Vertical resilient movement of the tool (μm)
m_S	Vertical resilient movement of the sample (μm)
δ_T	Initial slot for the tool (μm)
δ_S	Initial slot for the sample (μm)
τ	Slope of sample (mm/m)

1 Introduction

The surface roughness is an important factor, which can directly affect the integrity of the machined part, and regions of high surface roughness can initiate corrosion or increase surface adhesion. As being an ultimate aim of the operation, surface roughness-related variables need to be improved for longer service life of industrially important materials [1]. Meeting such expectation surface roughness depends on many factors that are related to the cutting parameters, machine setup, and the characteristics of the cutting tool [2]. One of the important factors affecting the surface condition resulting from the geometric and kinematic mapping and the effect of cutting speed is the phenomenon of minimum uncut chip thickness (MUCT). This is the uncut chip thickness (UCT) [3] value at which chip removal occurs [4, 5]. Specifications of MUCT are critical to avoid plowing effect and reduce residual stresses [6, 7]. Therefore, there has been a significant number of studies in the previous literature, which investigated the MUCT in micro-cutting operations for investigating its impact on the machinability characteristics. Wojciechowski [8] presents analysis of MUCT influence on surface roughness based on Brammertz approach [9] employed by the authors of [10, 11]. Mikolajczyk et al. [12] used Brammertz approach [9] to prepare software to visualization influence of MUCT on surface roughness for turning. Wu et al. [6] analyzed the effective rake angle using cutting force signal peaks. Their results showed that the MUCT caused higher cutting energy and poor surface quality as a result of plowing. Chen et al. [13] analyzed the cutting forces and surface quality to model chip shaping for predicting MUCT. Their findings showed that under certain cutting conditions, there is an optimum surface quality at which the plowing effect is eliminated. Chen et al. [14] performed surface quality analysis for chip thickness. An optimal solution-based work was carried out for minimal surface roughness. Yao et al. [7] studied the effect of plowing depth on residual stresses by developing a model using cutting forces and finite element simulation. The authors found that the energy accumulation on the surface of the body increased with the increase of plowing depth. Dib et al. [15] performed a study to determine the MUCT at the moment of chip formation during micro-end milling. The method proposed in this study allowed for the determination of MUCT along with an estimation of tool radius for monitoring the tool wear. Sahoo and Patra [16] developed a theoretical-mathematical model in micro-end milling considering tool run out, minimum chip thickness, and tooth-overlapping effects on the cutting forces and tool wear along with chip thickness. The results of their model showed good agreement with experimental findings on cutting forces. Sahoo et al. [17] carried out a study to determine the MUCT based on the ratio between MUCT and edge radius in micro-milling operations. Their results showed that high MUCT values produced curled and helical chips while using lower feed rates under MUCT produced irregular chips. Shi et al. [18] attempted to determine MUCT via acoustic emission signals with obtaining satisfactory surface quality during micro-end milling. Their procedure could be useful for surface quality analysis and optimization in a way that the prediction of MUCT using acoustic signals was found as a highly successful technique. Vipindas et al. [19] evaluated the cutting-edge radius effect in micro-end milling considering the chip thickness effect. They determined the critical threshold

for the feed rate value that can cause plowing. Xiong et al. [20] observed the chip formation mechanism according to tests and simulation during orthogonal cutting considering chip formation, shear plane, strain rate, and temperature. The authors indicated that comparative results of the test and finite element simulation were reliable when considering different cutting conditions. Molnar et al. [21] utilized a high-speed camera for recording the chip formation during orthogonal cutting under machine tool vibrations. Their aim was to determine the effect of cutting forces on chip thickness variation, surface quality, and stability of cutting direction. The findings of their investigation were used to evaluate models for shear angle and chip formation. Previous studies also investigated different aspects of MUCT during orthogonal cutting. Cutting using edge divide in orthogonal and oblique cutting depends on the value of inclination angle. Orthogonal cutting occurs for free cutting with $\lambda_s = 0°$ and was observed 2 components of forces [22]. Chip flow is perpendicular to cutting edge. Past studies used tools with a low value of inclination angle of cutting. Burak et al. [22] presented review of important articles on the mechanistics of orthogonal and oblique cutting. They present experimental results of oblique cutting for $\lambda_s = 7°$ and 11°.

Recently, a number of analyses have been published in the field of oblique cutting when the edge inclination angle (λ_s) is significantly different from 0° [23]. This angle is also known as the back rake angle (BR) since it has a strong influence on the cutting process [24].

Owing to the difference between orthogonal and oblique cutting in plastic flow throughout cutting-edge chip formation become distinctive [23, 25]. Liu et al. [26] found that for a three-dimensional orthogonal cutting process, the side flow effects can be eliminated by applying lower cutting speeds and a higher ratio between chip width and chip thickness. Fang [27] improved a model for oblique cutting to control chip flow direction and chip flow speed. Adibi-Sedeh et al. [28] performed an analysis to study the effects of using flat-faced nose radius tools for calculating the chip flow angle. Validation of the model was presented in the research. Similarly, a number of studies can be found in the open literature on mechanistic modeling of oblique cutting with different operating approaches. Jia et al. [29] performed sub-surface damage analysis using a three-dimensional oblique cutting model in machining to determine the optimum cutting parameters. Lotfi et al. [30] developed an oblique cutting theory for a friction model using three-dimensional turning operation based on measuring the cutting forces. Vinogradov [31] studied chip formation mechanisms during oblique cutting as orthogonal free cutting with a tool whose rake is a function of the face sharpening angle and cutting-edge inclination. Results of comparison between the calculated and experimental values of the forces showed a good fit. Liu et al. [32] modeled the cutting forces for analyzing the oblique cutting operation by taking into account the fracture toughness and thermo-mechanical properties of the material. Moufki et al. [33] presented a predictive theory of oblique cutting considering cutting forces in the view of the thermomechanical approach. Onozuka et al. [34] worked on the long oblique cutting edges during end milling operation for improving tool life, machining accuracy, and surface finish within the light of cutting forces and cutting temperatures. Lin et al. [35] also derived equations for modeling cutting forces for oblique milling operation. Ghosh et al. [36] performed and experimentally verified chip flow during oblique cutting by classifying the chip deviation by incorporating the effect of λ_s. Moufki et al. [37] were worked on thermomechanical modeling of oblique cutting operation, which allows for estimation of chip flow, contact length, and cutting forces. The developed model permits the prediction of the cutting forces, the chip flow direction, the contact length between the chip, and the tool and the temperature distribution. Wojciechowski [38] described the methods for the determination of MUCT via experimental, numerical, and analytical techniques during cutting with defined geometry tools. Presented methods concern mainly orthogonal turning. In [8], Wojciechowski presented more methods of experimental techniques of MUCT research. The previous research on the MUCT phenomenon was conducted mainly in the field of orthogonal cutting. The test results show the influence of the edge-rounding radius on the initiation of the cutting process and the formation of the chip. Mikolajczyk et al. present in [23] an analysis and research of the influence of the λ_s angle value on MUCT. The developed theory showed a decrease in MUCT with the increase of λ_s angle. The authors explain this by changing the configuration of the cutting-edge shape in the chip flow direction from the circular (orthogonal cutting) to the elliptical (oblique cutting). This theory was confirmed in research of MUCT for radial turning of C45 steel for $0° \le \lambda_s \le 60°$. In this work, the authors adopt the concept of Stabler [39] to determine the chip flow angle based on the edge inclination angle. It has been hypothesized that this influence also remains in the range of angles higher than those previously studied. Tools with high λ_s are not yet trading tools. Mikolajczyk et al. [40] present innovative tools for oblique cutting with $\lambda_s = 60°$. Was presented tools for external turning with straight and round cutting edge and tools for internal turning with round insert. Mikolajczyk et al. [41] present design and prototype special tool for oblique cutting with controlled inclination angle of cutting edge. Filippov [42] applied special cutting tools with round edge and $\lambda_s = 45°$ for developing an analytical model for calculating cutting-edge length in oblique cutting. Grzesik et al. [43] studied the use of an oblique tool

with a straight cutting edge and $\lambda_s = 55°$. Wojciechowski [8] in yours review paper describe results of authors paper [23] as an example of MUCT research in oblique cutting. Aydın and Köklü [44] developed a simulation technique based on arbitrary Lagrangian Eulerian to evaluate the performance of the finite element analysis approach. They indicated that proposed methodology was proactive way to improve the efficiency of the finite element simulation. Aydın and Köklü [45] used finite element analysis technique to evaluate the chip morphology and cutting forces in high speed machining of titanium based alloys. Milling force constants were analyzed in order to find the characteristics during cutting a hard material. Chip formation can be analyzed effectively to seek out the optimum chip type.

The purpose of this paper is to study the influence of oblique cutting conditions on MUCT phenomena for extremely high values of the inclination edge angle ($50° \le \lambda_s \le 85°$). This is important in understanding the cutting mechanism with a defined edge rounding in terms of extreme cutting-edge configurations. Section 2 presented the state of the art on λ_s angle and the effect of the rounding of the cutting edge on MUCT phenomenon. Section 3 provides details regarding the experimental setup and the measurement of $h_{\min}$ via machining tests. Section 4 presents the results and discussion of the machining experiment. Section 5 presented the conclusions from this study.

2 Theoretical aspects of inclination angle and rounding of cutting-edge effect on MUCT

The theory regarding the influence of λ_s on MUCT was elaborated in authors' study [23]. Fig. 1 shows 2D sketches of edge geometry in oblique cutting. Fig. 1a shows a view on the plane of cutting—Ps for the sample and rectilinear edge inclined to the main plane on λ_s (similarly, as presented in Sect. 3, Fig. 3). Fig. 1b shows the geometry of the real tool with a rounded edge—r_n. For the cutting edge presented in P_s plane, the location of the axes of Oxyz and Olmn systems is marked. The sections of edge in $P_o = P_f$ (Oxyz system) and Pn (Olmn system) can be also seen. Based on the analysis presented in our previous work on MUCT [23], it is critical to study the cutting-edge geometry in chip flow direction P_{cf} plane—that is associated with the cutting edge in Olmn system (Fig. 1b). In addition, the position of this plane is determined by the angle of chip flow η_{cf} [46, 47].

As previously discussed in the work of Mikołajczyk et al. [23], the angle of chip flow direction (η_{cf}) is related to λ_s by the following equation proposed by Stabler [39]:

$$\eta_{cf} = k.\lambda \tag{1}$$

where k is a dimensionless coefficient usually 0.8 to 1.

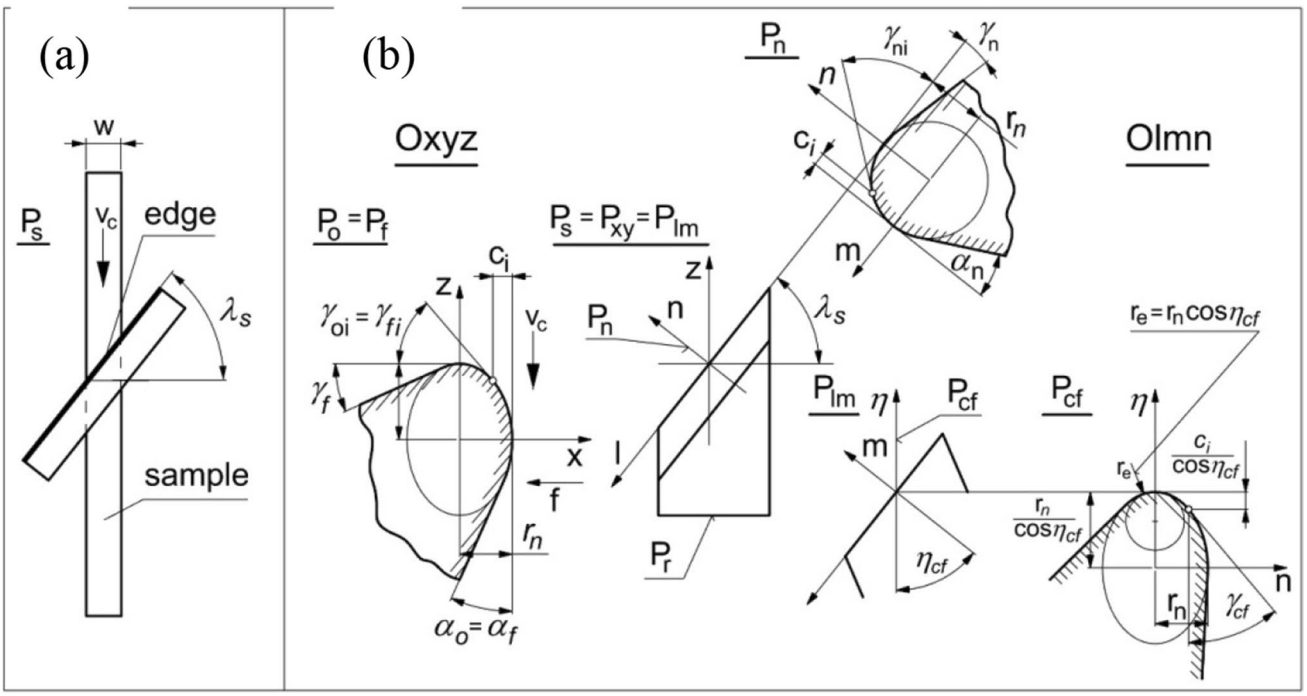

Fig. 1 2D sketch showing details of oblique cutting with round cutting edge: (**a**) view of oblique cutting process idea and (**b**) edge geometry for oblique cutting presented in a different section of Oxyz and Olmn systems (based on [23])

In P_{cf} direction, the round cutting-edge configuration was changed from a circle in the normal section (P_n plane) to an ellipse (Fig. 1b). Based on theory [48], it can be seen that the radius of the circle r_e is strictly tangential to the ellipse top. In the previous work of the authors, it was found that there is a sharp decrease in r_e with the increase of λ_s. Fig. 1b also showed the rake and clear angle for Oxyz and Olmn. The uncut chip thickness (UCT) is also denoted as c_i. The chip begins to form when UCT (c_i) reaches a value that defines the limit value of the rake angle (γ_{cfi}). At this instance, the value of MUCT $= h_{\min}$ is determined. Based on the theory presented in [23], the value γ_{cfi} angle can be obtained using $h_{\min}$ and $\eta_{cf} = k\lambda_s$ from equation:

$$\gamma_{cfi} = arctg[\frac{\left(r_n - h_{min}\right) * \cos\left(K\lambda_s\right)}{\sqrt{r_n^2 - \left(r_n - h_{min}\right)^2}}) \tag{2}$$

Also, based on the transformation of Eq. (2), $h_{\min}$ can be calculated for the known value of γ_{cfi} and $\eta_{cf} = k\lambda_s$ using the following equation:

$$h_{min} = r_n - \frac{r_n}{\sqrt{\left(\frac{cos^2(K\lambda_s)}{tan^2\gamma_{cfi}}\right) + 1}} \tag{3}$$

The square root in Eq. (3) makes it possible to obtain two values of $h_{\min}$. Only positive values of the solution make physical sense, and these are considered in the paper. In validation experiment [23] made for different values of r_n (18, 29, 90 µm) in terms of angles $0° \le \lambda_s \le 60°$, it was found that Eq. (3) adequately predicted the result of $h_{\min}$ with the increase of λ_s value for $k = 0.9$ (it was found for conditions of experiment). In the experiment presented in [23], the oblique cutting process was made in the radial free turning of C45 steel. This caused a certain variability of the rake and clear angles along the edge [23]. For planned cutting tests with $\lambda_s > 60°$, it is advisable to use a new technique of cutting to prevent changes in the geometry being observed in previous research [23]. Therefore, in the current study, the analysis involved studying the $h_{\min}$ phenomena for large values of λ_s in oblique cutting. The proposed research method as opposed to the previously used technique provides a constant rake angle along a straight cutting edge.

3 Materials and methods

3.1 Machine setup and testing technique

To verify the hypothesis on the effect of very large values of λ_s on MUCT ($h_{\min}$), a research setup was developed, which uses the milling machine feed as the cutting speed. Kinematics of cutting process corresponds to the technique of the planning process [49]. The tests were performed on a vertical milling machine, type FB 25 V NC (made in the Czech Republic Fig. 2a). The proposed technique ensures that the rake angle is kept constant along the straight edge (Fig. 2b). The samples were cut with a wide (w) rectilinear edge inclined at an angle λ_s to the cutting direction determined by the cutting speed vector (v_c). Free oblique cutting experiments were developed for constant position of the sample and the controlled edge position connected with its holder mounted in the stopped spindle (Fig. 2b). Due to the significant values of the λ_s, the relationship were developed for determining the edge length—l (Fig. 2c).

$$\mathrm{I} = w/cos\left(\lambda_s\right) \tag{4}$$

Presented graph (Fig. 2c) shows strong increase of cutting-edge length l for angle λ_s in terms of $\lambda_s = 75°\text{-}85°$. In view of the need to reasonably limit the length of cutting edge special samples with a width of 2.5 mm and edges with l = 30 mm were accepted for the tests. Samples for the experiment that was made of steel C45 are heavily used in many manufacturing companies and this material is from specific material list with guaranteed chemical structure and mechanical properties [50]. Chemical composition of C45 steel was presented in (Table 1). View of prepared sample is shown in Fig. 3.

The results of the $h_{\min}$ phenomena for oblique cutting presented in the analysis were used to develop the design of the edge for the tests [23]. The tool geometry was calculated based on the extreme value of clear angle α_o which changed with the increase of λ_s according to following developed equation:

$$\tan a_\circ = tan\ a_n.\cos\lambda_s \tag{5}$$

The value of α_o can be obtained from Eq. (5):

$$a_\circ = \mathrm{atan}(\tan a_n.\cos\lambda_s) \tag{6}$$

The form of the Eq. 6 is a simplification of the general solution due to the practical scope of α_o angle. Since the value of α_o is strongly depends on λ_s, special diagram is created (Fig. 4), which shows the influence of λ_s angle on clear angle α_o for different values of α_n in the normal section of edge. The geometry of the edge rake surface was adopted as the tool that was designed to test the initiation of the cutting process, which takes place at the rounded cutting edge. Therefore, $\gamma_{nN} = -30°$ was adopted, which was considered sufficient.

Based on presented analysis (Fig. 4), a cutting tool from HSS SW18 was fabricated with the following geometry: $\alpha_{nN} = 30°$ and $\kappa_{rN} = 90°$ (Fig. 5a). The rounding the cutting edge r_n was achieved by abrasive brushes. The measurements of r_n were carried out using a profilometer Hommel Tester T2000 (Hommel Werke Germany Fig. 5b).

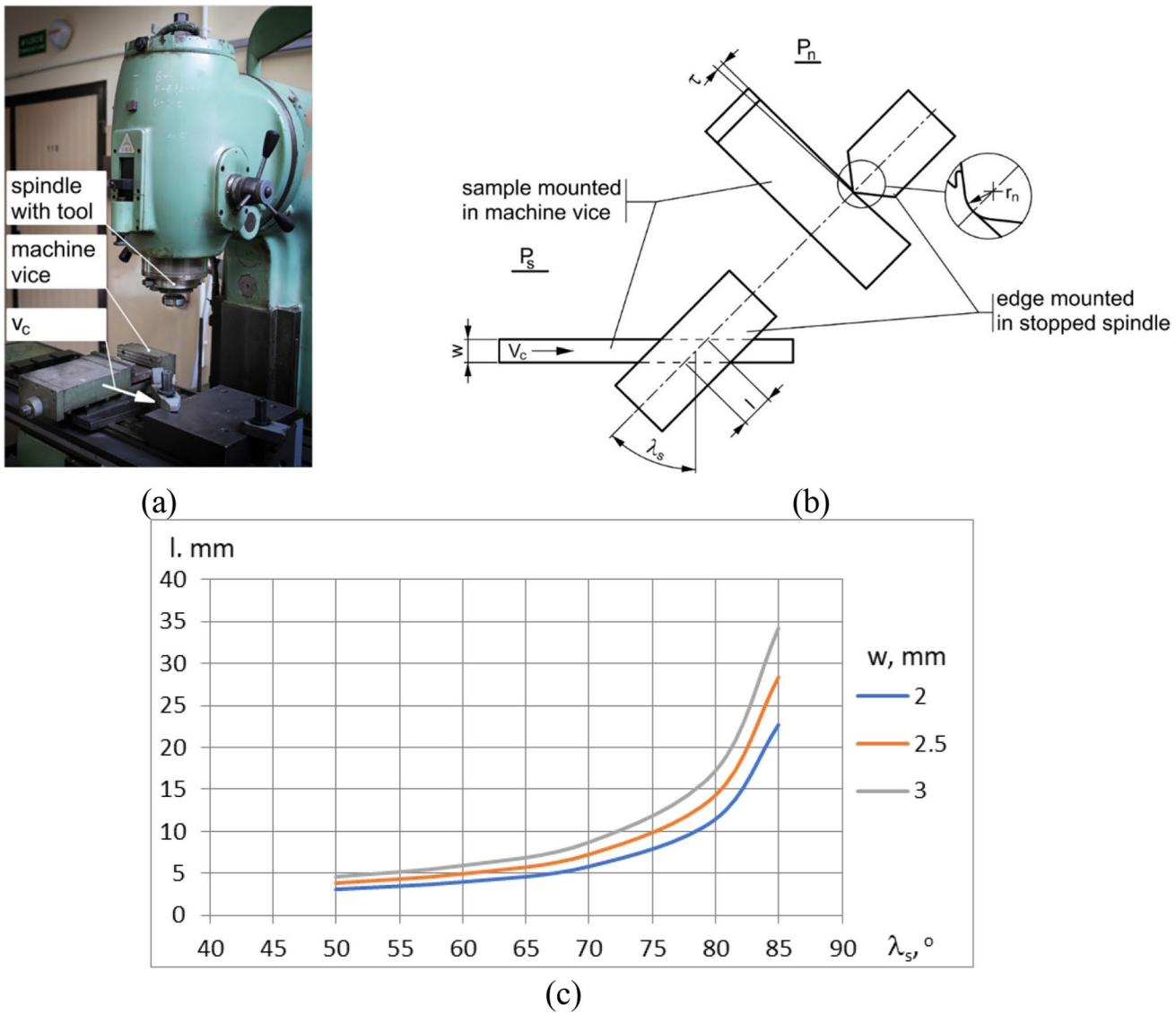

Fig. 2 View of (**a**) the FB25VNC milling machine tool used in the tests, (**b**) kinematics of free oblique cutting experiments using mill machine tool and sample set in the direction of feed (v_c) and the edge mounted at the angle λ_s in the stopped spindle, and (**c**) influence of λ_s value on cutting edge length l for different value of sample width w

Table 1 C45 steel chemical composition

Material	Microstructure	Chemical composition %					
C45	Perlite + ferrite	C	Mn	Si	Cr	Ni	S
		0.45	0.65	0.25	0.20	0.20	0.04

The profilograms were made using that same vertical and horizontal zoom and repeated in different places 6 times. The mean value of the measurements of rounding the cutting edge was determined $r_n = 185$ µm. Surfaces of samples (Fig. 3) using grinding process were prepared ($R_a = 0.32$ µm), for achieve repetitive conditions for all attempts. Surface roughness of sample was measured using ISO 4287 standard.

The edge (Fig. 5a) was placed in a special holder (Fig. 5c and 5d) and was mounted in the milling spindle chuck.

The milling spindle is stopped and a tool allowing accurate positioning relative to the sample. The λ_s angle was carried out by turning the tool in the spindle and was set using a workshop protractor with a magnifying glass MKMb 315. Samples (see Fig. 3) were inclined relative to the table plane

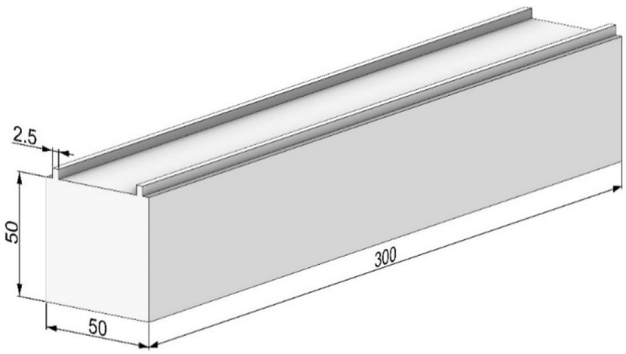

Fig. 3 View of prepared sample for oblique cutting experiment

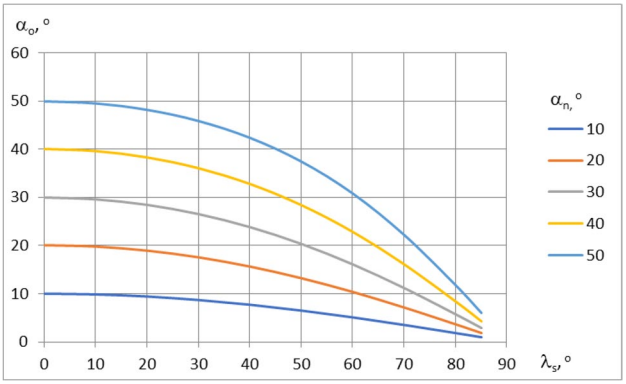

Fig. 4 Influence of λ_s angle on clear angle α_o value for different values of α_n

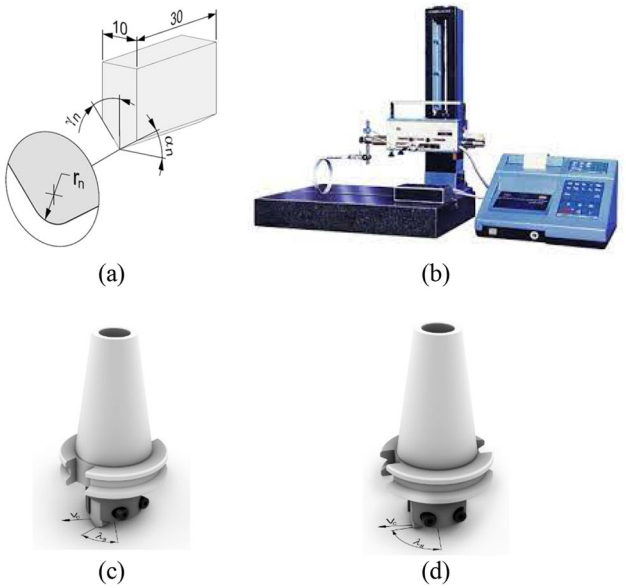

Fig. 5 View of (**a**) edge used in the experiment (γ_n = -30°, α_n = 30°, r_n = 185 µm), (**b**) Hommel Tester T2000 (Hommel Werke, Germany) used in research, (**c**) an example of the setting of the holder for fixing the edge λ_s = 50°, and (**d**) an example of the setting of the holder for fixing the edge λ_s = 80°

Table 2 Machining conditions and tool geometry specifications

Workpiece material	C45
Machining operation	Free planning with SW18 tool
Rake angle, γ_{nN} (°)	-30
Clear angle, α_{nN} (°)	30
Major edge angle, κ_{rN} (°)	90
Cutting speed, v_c (m/min)	0.063

on τ to obtain the effect of vertical feed with high accuracy. Sample alignment was carried out using a digital sensor with an accuracy of 1 µm. This was achieved by clamping the sample in a vise mounted on a milling table (see Fig. 2a). In the used technique, the vertical feed of the tool f_v depends on the v_c and the τ inclination of the sample (see Fig. 2b).

Machining conditions and tool geometry specifications are presented in Table 2.

3.2 Measurement of hmin

During the cutting process, in the case of the adopted model for testing, we observed the stress–strain behavior of the workpiece material (Fig. 6).

There are three consecutive phases of the workpiece behavior which can be seen in Fig. 6a:

1. **a**—elastic deformations
2. **b**—elastic and plastic deformations
3. **c**—chip formation—cutting, elastic, and plastic deformation

In **a** phase due to the occurrence of elastic deformations of the workpiece material flowing onto the cutting edge is plowed under the tool flank face [8]. In this phase, the workpiece is only subjected to elastic deformation and returns to the nominal position after the tool passes.

In **b** phase when UCT value is lower than $h_{\min}$ causes the formation of elastic–plastic and plastic deformations of the workpiece. The result is the formation of a plastic flash, which, however, is not transformed into a chip [8].

In **c** phase when increase UCT to the value within the range $h \geq h_{\min}$ induces the cutting process and chip formation [8, 23].

The main challenge was to determine the moment at which the chip begins to form. MUCT ($h_{\min}$) was indicated mating of surface accompanying the chips formation after tool sliding on the work surface (gloss appears) [23]. The method of solving this problem was presented in a previous study [23] but it cannot be used in the current work due to using a different cutting model (free cutting—no flashing).

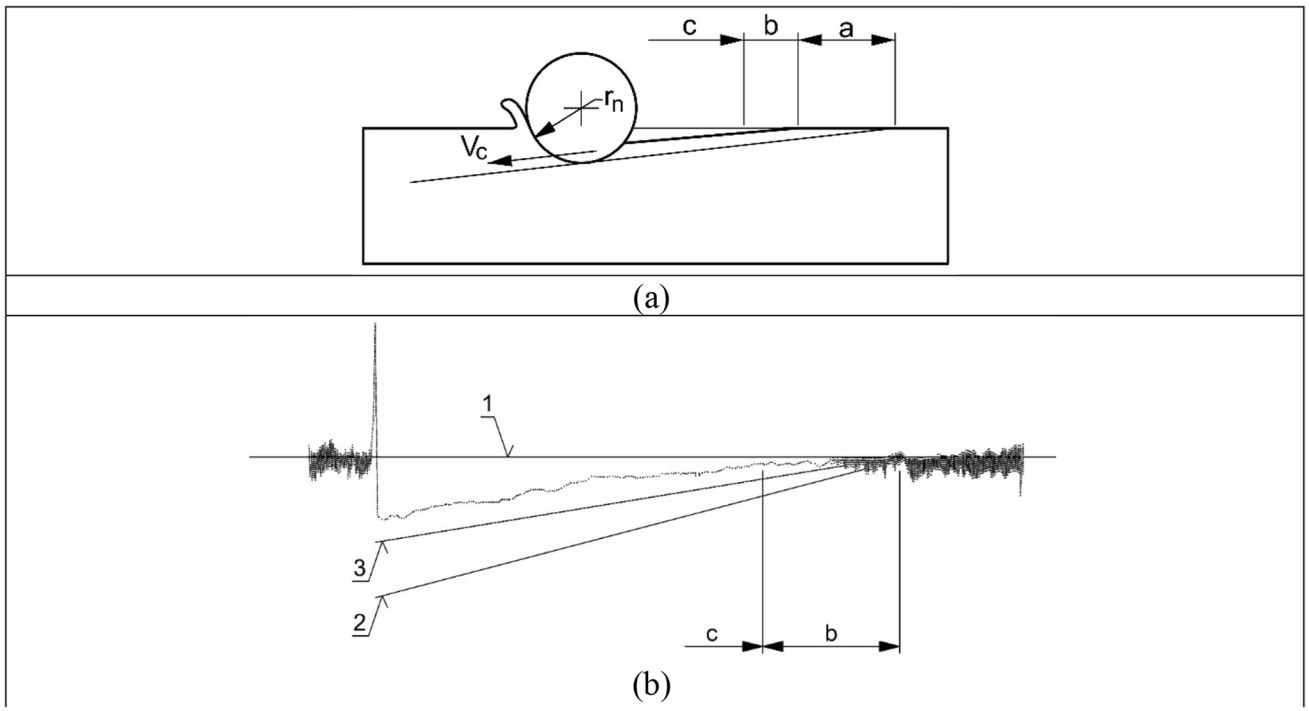

Fig. 6 2D sketch showing (**a**) phases of cutting process initiation: a—sliding phase gloss surface, b—initiation of cutting process phase matt surface, and c—the cutting process with chip constitution; (**b**) example profilogram of the sample surface: 1—sample surface line, 2—tool theoretical path, and 3—actual tool path including machine tool deformations

An original method of determining the moment of transition from plastic deformation to cutting was adopted, consisting of the analysis of the profilogram made in the cutting direction (Fig. 6b). In addition, the profilometer was used to record the registration of surface profile.

Because the cutting forces appeared to be quite high in combination with the machine rigidity, which could disturb the results of the cutting tests (measurements of the order of several micrometers), a system was used during the tests to record the elastic deformation of the main part of machine tool, which were taken into account when calculating $h_{\min}$, as shown in Fig. 7.

Then, based on the analysis of profilogram from each cutting test and deformation measurements results using the setup shown in Fig. 7, similar as in [23] h_r was determined using the following equation:

$$h_r = h - m_T - m_s \tag{7}$$

In this case, the vertical movement elements of cutting zone of tool m_T and sample m_S were considered. In this way, the actual UCT value of h_r can be read off with a high degree of accuracy.

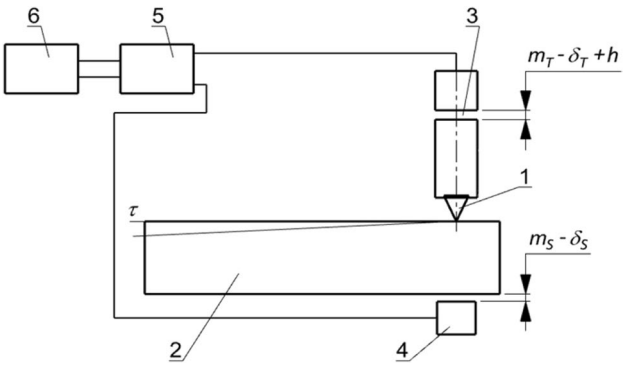

Fig. 7 Test bench scheme based on [23]: 1—tool, 2—sample, 3—tool sensor (IWT302), 4—sample sensor (IWB201), 5—measuring instrument UM131 (Germany), and 6—recorder M3273 (Russia)

3.3 Plan of experiment

For the experiment, constant factors such as workpiece material, edge geometry, and machining parameters such as cutting speed and feed rate were used [8, 23]. The cutting speed was derived from the process modeling technique used on the mill tool machine. The feed rate was provided by setting up the sample for high accuracy of the chip initiation process. The variable factor in the study was the inclination angle of edge λ_s.

Table 3 Plan of experiment (constant parameters: dry cutting of C45 steel, $r_n = 185$ µm, $v_c = 0.063$ m/min, and $f_v = 37.8–53.5$ µm/min)

No	Inclination edge angle, λ_s (°)
1	50
2	60
3	70
4	80
5	85

Table 4 Results of experiment

No	Inclination edge angle, λ_s (°)	MUCT, h_{min} (µm)
1	50	12.0
2	60	9.0
3	70	7.0
4	80	5.0
5	85	4.0

The samples were machined using along feed of mill machine table $f = 63$ mm/min and $v_c = 0.063$ m/min. Vertical feed of edge f_v was determined by association on the applied sample slope ($\tau = 0.60–0.85$ mm/m) and cutting speed v_c. Based on used cutting speed and sample slope, the vertical feed f_v was calculated using equation below:

$$f_v = \frac{\tau}{v_c} \tag{8}$$

After substituting the used to Eq. 8 τ inclination, it was found that $f_v = 0.0378 – 0.0535$ m/min. Because these are very low values, it can be presented as $f_v = 37.8–53.5$ µm/min. The edge was set at 30 µm from the surface to ensure that the tool contact with the surface was achieved after a displacement of approximately 50–35 mm, depending on the τ inclination of the specimen. The distance was set using an optical method and controlled with a slit gage (Vogel, Germany). Next, λ_s inclination angle is set. Once the tool had been locked in place, the machining process begins by switching on the feed rate. The cutting process was stopped after a certain pre-determined machining time until the cutting initiation occurred. A profilogram was taken of the machined specimen and from this, based on the observation of the effect of the cutting process on profilogram (Fig. 6b) the nominal chip thickness h was determined. Next based on measuring the tool m_T and the sample m_S vertical resilient movement as shown in Fig. 7, the h_{min} value was calculated using Eq. 7. The trials for each inclination angle value were repeated three times. The tests were carried out for large values of the inclination angle $50° \le \lambda_s \le 85°$. The plan of experiments is presented in Table 3

4 Results and discussion

4.1 Results of experiments

Table 4 shows the results of MUCT according to different λ_s ranging from 50° to 85°. For $\lambda_s = 50°$ was achieved $h_{min} = 12$ µm, and for $\lambda_s = 85°$ was obtained $h_{min} = 4$ µm. The results show the relationship between λ_s and MUCT is approximately inversely proportional. Increasing λ_s by 35° resulted in up to threefold reduction in h_{min} value clearly shows the very significant impact of λ_s on MUCT.

4.2 Prediction of hmin based on theory [23]

Results of experiment presented in Table 4 were used for found parameters of oblique cutting process: γ_{cf} angle and k parameter based of Eq. 2 and Eq. 3 from theory elaborated by authors [23]. The calculations were performed using the least-squares method (LSM) to obtain the lowest value of the mean square deviation (MSD). To Eq. 2, the experimental values of h_{min} and successively different values of the k-factors ($k = 0.65$, 0.70, 0.75, 0.80, and 0.85) for calculate η_{cf} were substituted. For each λ_s value, the values of γ_{cf} were determined in this way. For these values, the mean was determined and for successive λ_s angles the square deviation was determined. The smallest error was obtained for $k = 0.75$ as shown in Table 5 and Fig. 8a. The theoretical values of the angles γ_{cf} for $k = 0.75$ was determined as presented in Table 5 and

Table 5 Results of calculation of γ_{cf} and LSM for $k = 0.75$

No	λ_s (°)	h_{min} (µm)	k	η_{cf} (°)	γ_{cf} (°)	LSM
1	50	12	0.75	37.5	64.51	0.110153
2	60	9	0.75	45,0.0	-65.43	0.348108
3	70	7	0.75	52.5	-65.10	0.065129
4	80	5	0.75	60.0	-64.66	0.033272
5	85	4	0.75	63.75	-64.51	0.109503
					-64.84	**0.133233**

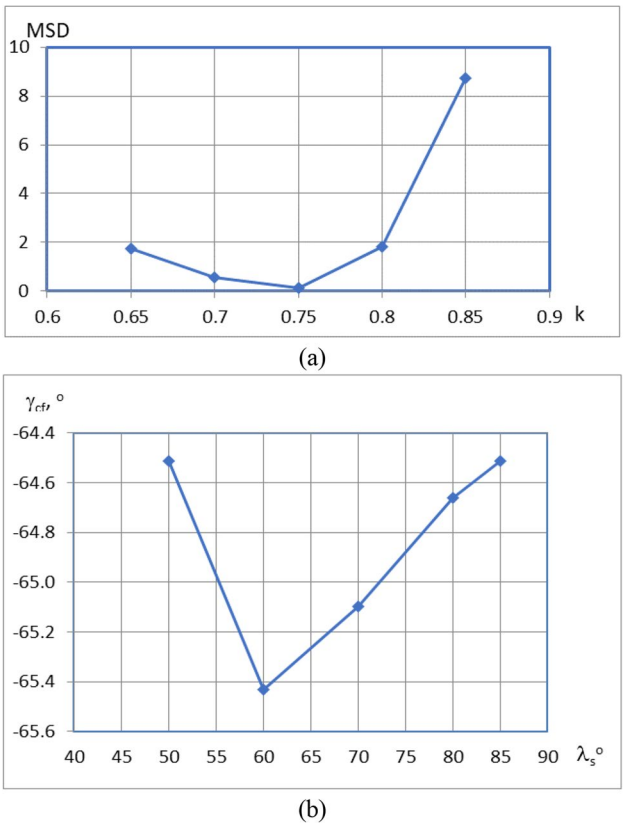

Fig. 8 Results of calculation: (**a**) influence of k value on the mean square error of γ_{cf} determination and (**b**) values of γ_{cf} angle for $k=0.75$ using of Eq. 2

shown in Fig. 8b. The optimization procedure yielded results in the range η_{cf}=-64.51° to -65.43°. In further calculations, the mean value γ_{cf}=-64.8° was used for the test conditions.

Table 6 shows a comparison of the theoretical and experimental values of $h_{\min}$ based on approximation of results using Eq. 3 for $\eta_{cf}=0.75\ \lambda_s$ and γ_{cf}=-64.8°. Table 6 also shows the predicted $h_{\min}$ values calculated using Eq. 3 for $0° \le \lambda_s \le 40°$ an extrapolation of results of experiments prepared for area our previous research [23]. The comparison of the experimental MUCT with the theoretically predicted ones based on Eq. 3 is presented in Fig. 9. Extrapolation of predicted results of $h_{\min}$ for $0° \le \lambda_s \le 40°$ is signed using dashed lines. In Fig. 9, it can be seen that the $h_{\min}$ values determined theoretically from Eq. 3 based on the parameters obtained by the optimization procedure coincide with the experimental results. This confirms the theory presented in the paper [23]. The extrapolation results for the obtained parameters show an increase in the $h_{\min}$ value with a decrease in the value of the angle λs. However, this change is not as pronounced as for the experimental range. The presented graph indicates that in the range of significant values of the angle λs, very significant changes in the mechanics of the cutting process occur, especially in the MUCT range.

4.3 Analysis of cutting edge section in the chip flow direction

Experimental results and analyses, based on the theoretical model [23], are related to the geometry of the cutting edge in the P_{cf} section (Fig. 1). In chip flow direction the circular contour of edge for $\lambda_s=0°$ changes into an elliptical for $\lambda_s>0°$. The contour of the ellipse depends on the angle of chip flow η_{cf}. It was found that in when calculating $h_{\min}$, coefficient $k=0.75$ was used for the calculation of η_{cf} value. Based on this, the values for the ellipse half-axes were calculated. Taking into account that $A=r_n$, $B=r_n/\cos\eta_{cf}$ (Fig. 1), the influence of λ_s for $\eta_{cf}=0.75\lambda_s$ is given in Table 7. Also based on chip flow direction, the radius r_e was strictly a tangential circle to the ellipse top [46] and was calculated using the equation presented in Fig. 1.

The changes in the shape of the cutting edge drawn based on data from Table 7 are visualized in Table 8. In Fig. 10

Table 6 Comparison of results of theoretical and experimental $h_{\min}$ values based on approximation of results of research using Eq. 3 for $\eta_{cf}=0.75\ \lambda_s$ and $\gamma_{cf}=-64.80°$

λ_s (°)	k	η_{cf} (°)	γ_{cf} (°)	MUCT, $h_{\min}$ (μm)		
				Theoretical	Experimental	LSM
0	0.75	0.00	-64.80	17.65		
10	0.75	7.50	-64.80	17.39		
20	0.75	15.00	-64.80	16.63		
30	0.75	22.50	-64.80	15.38		
40	0.75	30.00	-64.80	13.72		
50	0.75	37.50	-64.80	11.72	12.00	0.077975
60	0.75	45.00	-64.80	9.50	9.00	0.245393
70	0.75	52.50	-64.80	7.18	7.00	0.032937
80	0.75	60.00	-64.80	4.94	5.00	0.003585
85	0.75	63.75	-64.80	3.90	4.00	0.009815
						0.073941

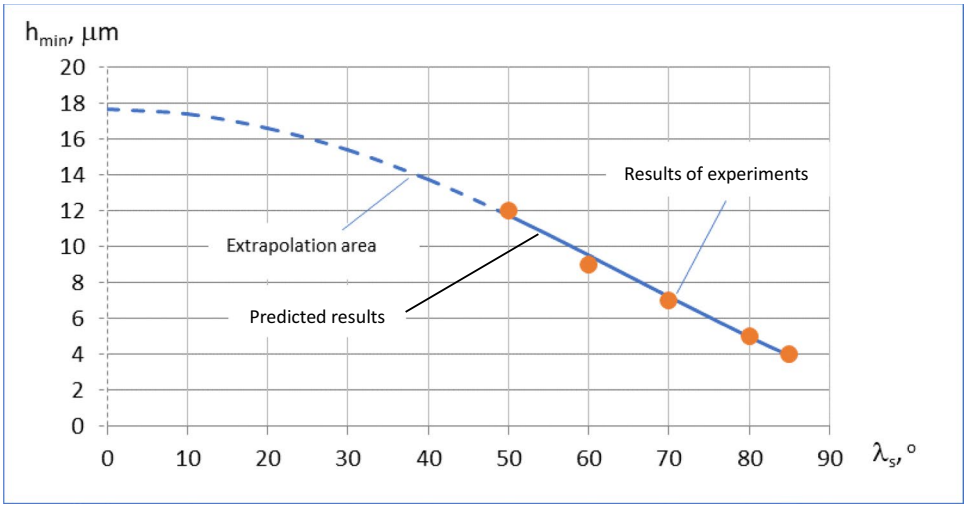

Fig. 9 Comparison of MUCT experimental results with theoretically predicted values based on Eq. 3 for $k=0.75$ and mean value of the angle γ_{cf}= -64.8°

Table 7 Influence of inclination angle λ_s for $\eta_{cf}=0.75\lambda_s$ on values of A and B axes of the ellipse and r_e radius

λ_s (°)	η_{cf} (°)	A (mm)	B (mm)	r_e (µm)
0	0.00	185.00	185.00	185.00
50	37.50	185.00	233.13	146.81
60	45.00	185.00	261.53	130.87
70	52.50	185.00	303.71	112.69
80	60.00	185.00	369.66	92.59
85	63.75	185.00	417.80	81.92

was presented comparison of the theoretical values of $h_{\min}$ and shape of cutting edge in P_{cf} section for orthogonal and oblique cutting for γ_{cf}= -64.8°.

As presented in Table 3, it is possible to determine $h_{\min}$ using Eq. (3), based on the γ_{cf} angle and η_{cf}, $h_{\min}$ value adequately to the edge curvature, which significantly change as it can be seen from the comparison presented in Table 8.

However, the observed change in $h_{\min}$ is much larger than the observed change of circle radius strictly tangential to top of ellipse r_e. For example, for $\lambda_s=50°$, $h_{\min}=12$ µm was obtained and for $\lambda_s=85°$, $h_{\min}=4$ µm was found, i.e., a decrease of 3 times, while the radius $r_e=146.81$ µm for $\lambda_s=50°$ and $r_e=81.92$ µm for $\lambda_s=85°$, i.e., they decreased by less than 2x. This is since $h_{\min}$ is governed by the angle γ_{cf} which is found on the curvature of the ellipse. In Fig. 10, the theoretical values of $h_{\min}$ are presented for $\lambda_s=50°$

Table 8 View of edge shape and circle strictly tangential to an ellipse in P_{cf} section defined for chip flow angle ηcf =k.λs when k=0.75

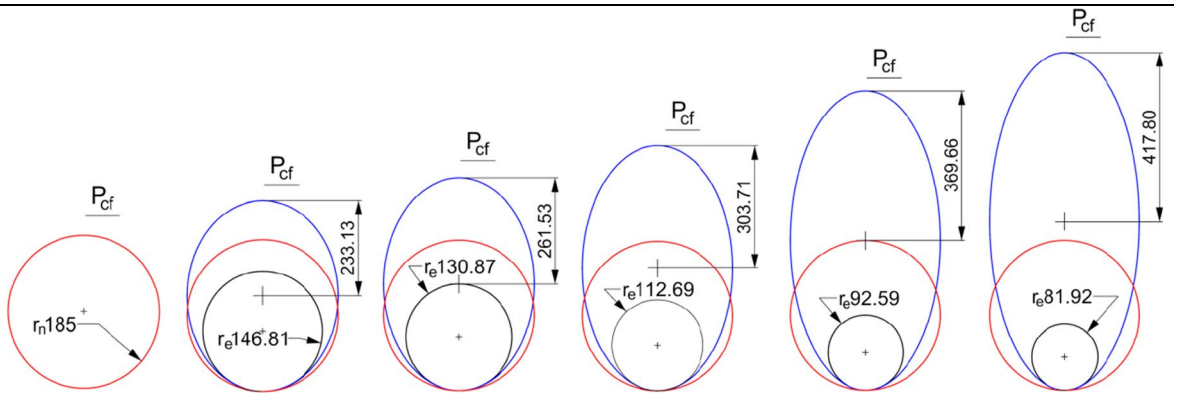

λ_s (°)	0	50	60	70	80	85
η_{cf} (°)	0	37.5	45	52.5	60	63.75
r_e (mm)	185	146.81	127.33	112.69	92.59	81.92
$h_{\min}$ (µm)	17.65	11.72	9.50	7.18	4.94	3.90

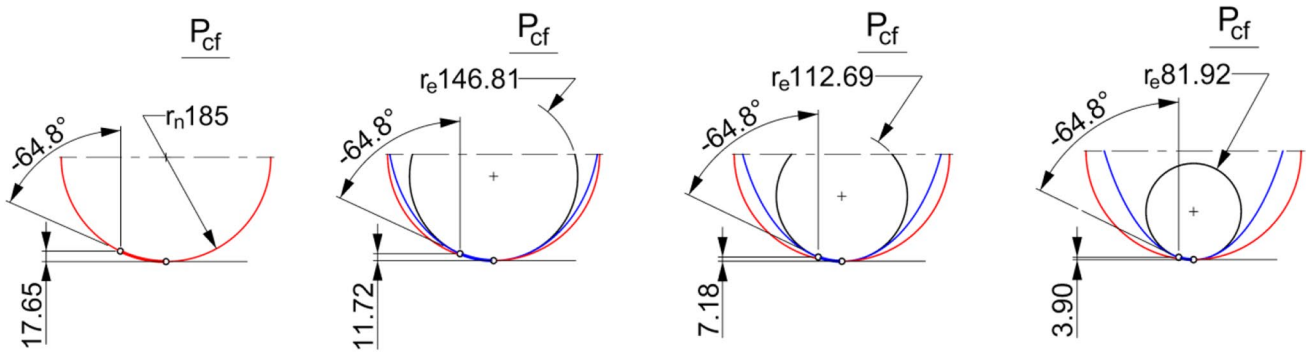

Fig. 10 Comparison of the theoretical values of h_{min} in P_{cf} section for orthogonal cutting: (**a**) $\lambda_s = 0°$, and oblique cutting: (**b**) $\lambda_s = 50°$, (**c**) $\lambda_s = 70°$, (**d**) $\lambda_s = 85°$ for γ_{cf}=-64.8°, and $\eta_{cf} = 0.75\ \lambda_s$

and 70° and $\lambda_s = 85°$ and also to comparison for $\lambda_s = 0°$. The predicted value of h_{min} for $\lambda s = 0°$ derived from Eq. 3 is17.65 µm, which corresponds to the value of $h_{min}/r_n = 0.1$ often found in the research of h_{min} for orthogonal cutting. Thus, for very high values of λ_s under the current experiments, the MUCT value is more than four times smaller. In oblique cutting, the h_{min} was significantly reduced compared to orthogonal cutting.

4.4 System of cutting process regulation of MUCT in oblique cutting

Results of experiments and its analysis based proposed theory show that for the defined edge (r_n), one material and value of cutting speed we can get values of: γ_{cf} angle and k coefficient of chip flow direction, which solve problem of prediction h_{min}. Based on results of research and analysis using of proposed theory [23] was proposed system of cutting process regulation of MUCT in oblique cutting (Fig. 11).

Figure 11 presents diagram of cutting process regulation when λ_s was changed and influenced on η_{cf} angle based on k value, which defined stereometry of cutting edge with r_n value and predicted using Eq. 3 h_{min} based on obtained γ_{cfi} and k values for experimental conditions. Results of presented research confirm the statement from previous literature [23] which states that for a tool with a specific r_n radius, the reduction in h_{min} value with the increase of λ_s to 60° is also confirmed in the extremely high values of λ_s (up to 85°).

The presented result of this research supports these possibilities, which can be also applied for very high values of the λ_s angles which are not else used in practice. The results confirmed the significant lowering h_{min} value with the increase of λ_s angle opens the possibility of developing new tools [40, 41] for finish machining in the field of oblique cutting. These tools can be designed and manufactured using market inserts [40, 41]. Presented result open new subject of research improve surface quality based on lowering of h_{min} value which influenced on surface roughness [8, 12]. Also, it is possible to explain some issues of surface wear in the process of friction [51].

5 Conclusions

The current work investigated the MUCT h_{min} in oblique cutting process of C45 steel, for extremely high value of edge inclination angle λ_s, in research was used special technique based on milling tool machine using a special tool

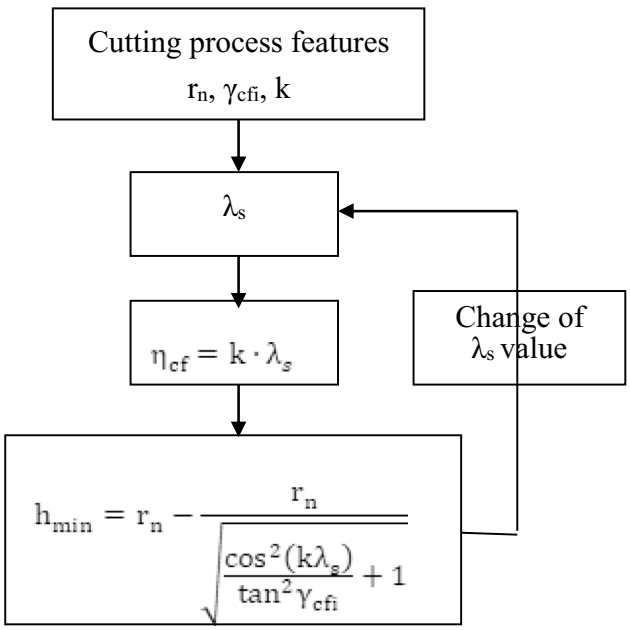

Fig. 11 System of cutting process regulation of MUCT in oblique cutting

and sample. Enabled model tests in the unprecedented range of angles λ_s not used in research to date. This is novelty of presented article.

According to the results from this study and results of previous presented authors article paper [23], the following conclusions were made:

- In experimental studies made using tool with $r_n = 185$ µm, it was found that in the range of angles $50° \le \lambda_s \le 85°$ significantly decrease the MUCT value from $h_{\min} = 12$ µm for $\lambda_s = 50°$ to $h_{\min} = 4$ µm for $\lambda_s = 85°$. Increasing λ_s by 35° resulted in up to threefold reduction in MUCT
- Analyses of the experimental results of $h_{\min}$ for used λ_s angle confirmed authors theory [23]. With use of Eq. (3) was determined chip flow angle coefficient $k = 0.75$ and critical value of rake angle $\gamma_{cf} = -64.8°$ based LSM. This provides prediction of results with great accuracy to experimental value
- Analysis of shape cutting edge in chip flow direction show that on cutting process influenced critical value of rake angle
- The applied test technique, using mill tool machine with compensation for the effects of deformation, allows for a sufficiently precise determination of the $h_{\min}$ based on profilograms analyses. Used cutting method limits cutting speed range to a very low value
- Practical effect of presented research is opening the possibility of developing new tools for finish machining in the field of oblique cutting with high values of λ_s angle [40, 41]
- Presented results open new subject of research possibility to improve surface quality based on lowering of MUCT effect on surface roughness [8, 12]. Also, it is possible to explain some issues of surface wear in the process of friction [51]

Funding No funding was received for conducting this study.

Data availability The data used in this work can be requested by contacting the first author.

Code availability Not applicable.

Declarations

Ethics approval Not applicable.

Consent to participate Not applicable.

Consent for publication Not applicable.

Competing interests The authors declare no competing interests.

References

1. Arrazola P et al (2013) Recent advances in modelling of metal machining processes. CIRP Ann 62(2):695–718
2. Zhuang K, Fu C, Weng J, Hu C (2021) Cutting edge microgeometries in metal cutting: a review. Int J Adv Manuf Technol 116(7):2045–2092. https://doi.org/10.1007/s00170-021-07558-6
3. Kouravand S, Imani BM (2014) Developing a surface roughness model for end-milling of micro-channel. Mach Sci Technol 18(2):299–321. https://doi.org/10.1080/10910344.2014.897846
4. Bergmann B, Denkena B, Grove T, Picker T (2019) Chip formation of rounded cutting edges. Int J Precis Eng Manuf 20(1):37–44. https://doi.org/10.1007/s12541-019-00020-4
5. Ulutan D, Sima M, Özel T (2011) Prediction of machining induced surface integrity using elastic-viscoplastic simulations and temperature-dependent flow softening material models in titanium and nickel-based alloys. Adv Mater Res Trans Tech Publ. https://doi.org/10.4028/www.scientific.net/AMR.223.401
6. Wu X, Liu L, Du M, Shen J, Jiang F, Li Y, Lin Y (2020) Experimental study on the minimum Undeformed Chip thickness based on effective rake angle in Micro milling. Micromachines 11(10):924. https://doi.org/10.3390/mi11100924
7. Yao Y, Zhu H, Huang C, Wang J, Zhang P, Yao P, Wang X (2020) Determination of the minimum chip thickness and the effect of the plowing depth on the residual stress field in micro-cutting of 18 Ni maraging steel. Int J Adv Manuf Technol 106(1):345–355. https://doi.org/10.1007/s00170-019-04439-x
8. Wojciechowski S (2021) Estimation of minimum uncut chip thickness during precision and micro-machining processes of various materials—a critical review. Materials 15(1):59. https://doi.org/10.3390/ma15010059
9. Brammertz P (1961) Die entstehung der oberflächenrauheit beim feindrehen. Ind Anz 2:25–32
10. Schultheiss F, Hägglund S, Bushlya V, Zhou J, Ståhl J-E (2014) Influence of the minimum chip thickness on the obtained surface roughness during turning operations. Procedia Cirp 13:67–71. https://doi.org/10.1016/j.procir.2014.04.012
11. Wojciechowski S, Nowakowski Z, Majchrowski R, Królczyk G (2017) Surface texture formation in precision machining of direct laser deposited tungsten carbide. Adv Manuf 5(3):251–260. https://doi.org/10.1007/s40436-017-0188-3
12. Mikolajczyk, T. Modeling of minimal thickness cutting layer influence on surface roughness in turning. in Appl Mech Mater 2014. Trans Tech Publ. https://doi.org/10.4028/www.scientific.net/AMM.656.262
13. Chen N, Chen M, Wu C, Pei X, Qian J, Reynaerts D (2017) Research in minimum undeformed chip thickness and size effect in micro end-milling of potassium dihydrogen phosphate crystal. Int J Mech Sci 134:387–398. https://doi.org/10.1016/j.ijmecsci.2017.10.025
14. Chen N, Chen M, Wu C, Pei X (2017) Cutting surface quality analysis in micro ball end-milling of KDP crystal considering

size effect and minimum undeformed chip thickness. Precis Eng 50:410–420. https://doi.org/10.1016/j.precisioneng.2017.06.015
15. Dib M, Duduch J, Jasinevicius R (2018) Minimum chip thickness determination by means of cutting force signal in micro endmilling. Precis Eng 51:244–262. https://doi.org/10.1016/j.precisioneng.2017.08.016
16. Sahoo P, Patra K (2018) Mechanistic modeling of cutting forces in micro-end-milling considering tool run out, minimum chip thickness and tooth overlapping effects. Mach Sci Technol. https://doi.org/10.1080/10910344.2018.1486423
17. Sahoo P, Patra K, Szalay T, Dyakonov AA (2020) Determination of minimum uncut chip thickness and size effects in micro-milling of P-20 die steel using surface quality and process signal parameters. Int J Adv Manuf Technol 106(11):4675–4691. https://doi.org/10.1007/s00170-020-04926-6
18. Shi Z, Li Y, Liu Z, Qiao Y (2018) Determination of minimum uncut chip thickness during micro-end milling Inconel 718 with acoustic emission signals and FEM simulation. Int J Adv Manuf Technol 98(1–4):37–45. https://doi.org/10.1007/s00170-017-0324-z
19. Vipindas K, Anand K, Mathew J (2018) Effect of cutting edge radius on micro end milling: force analysis, surface roughness, and chip formation. Int J Adv Manuf Technol 97(1):711–722. https://doi.org/10.1007/s00170-018-1877-1
20. Xiong Y, Wang W, Jiang R, Lin K, Shao M (2018) Mechanisms and FEM simulation of chip formation in orthogonal cutting in-situ TiB2/7050Al MMC. Materials 11(4):606. https://doi.org/10.3390/ma11040606
21. Molnar TG, Berezvai S, Kiss AK, Bachrathy D, Stepan G (2019) Experimental investigation of dynamic chip formation in orthogonal cutting. Int J Mach Tools Manuf 145:103429. https://doi.org/10.1016/j.ijmachtools.2019.103429
22. Aksu B, Çelebi C, Budak E (2016) An experimental investigation of oblique cutting mechanics. Mach Sci Technol 20(3):495–521. https://doi.org/10.1080/10910344.2016.1196458
23. Mikołajczyk T, Latos H, Pimenov DY, Paczkowski T, Gupta MK, Krolczyk G (2020) Influence of the main cutting edge angle value on minimum uncut chip thickness during turning of C45 steel. J Manuf Process 57:354–362. https://doi.org/10.1016/j.jmapro.2020.06.040
24. Coromant S (1994) Modern metal cutting: a practical handbook. Sandvik Coromant
25. Arrazola P-J, Attia H, Melkote SN, M'Saoubi R, Outeiro J, Rech J, Saldana C, Schulze V, Grzesik W (2017) Advances in material and friction data for modelling of metal machining. Cirp Annals-Manufacturing Technology 66(2). https://doi.org/10.1016/j.cirp.2017.05.002
26. Liu R, Eaton E, Yu M, Kuang J (2017) An investigation of side flow during chip formation in orthogonal cutting. Procedia Manuf 10:568–577. https://doi.org/10.1016/j.promfg.2017.07.053
27. Fang N (1998) An improved model for oblique cutting and its application to chip-control research. J Mater Process Technol 79(1–3):79–85. https://doi.org/10.1016/S0924-0136(97)00385-3
28. Adibi-Sedeh A, Madhavan V, Bahr B (2002) Upper bound analysis of oblique cutting with nose radius tools. Int J Mach Tools Manuf 42(9):1081–1094. https://doi.org/10.1016/S0890-6955(02)00007-X
29. Jia Z-y, Chen C, Wang F-j, Ma J-w, Yang F (2018) Three-dimensional oblique cutting model for sub-surface damage analysis in CFRP/Ti stack composite machining. Int J Adv Manuf Technol 96(1):643–655 https://doi.org/10.1007/s00170-018-1626-5
30. Lotfi M, Amini S, Sajjady SA (2019) Development of a friction model based on oblique cutting theory. Int J Mech Sci 160:241–254. https://doi.org/10.1016/j.ijmecsci.2019.06.038
31. Vinogradov A (2014) On the mechanism of chip formation in oblique cutting of metals. J Superhard Mater 36(6):428–434. https://doi.org/10.3103/S1063457614060094
32. Liu C, Wang G, Ren C, Yang Y (2014) Mechanistic modeling of oblique cutting considering fracture toughness and thermomechanical properties. Int J Adv Manuf Technol 74(9–12):1459–1468. https://doi.org/10.1007/s00170-014-6100-4
33. Moufki A, Dudzinski D, Le Coz G (2015) Prediction of cutting forces from an analytical model of oblique cutting, application to peripheral milling of Ti-6Al-4V alloy. Int J Adv Manuf Technol 81(1):615–626. https://doi.org/10.1007/s00170-015-7018-1
34. Onozuka H, Utsumi K, Kono I, Hirai J, Numata Y, Obikawa T (2015) High speed milling processes with long oblique cutting edges. J Manuf Process 19:95–101. https://doi.org/10.1016/j.jmapro.2015.06.004
35. Lin B, Wang L, Guo Y, Yao J (2016) Modeling of cutting forces in end milling based on oblique cutting analysis. Int J Adv Manuf Technol 84(1–4):727–736. https://doi.org/10.1007/s00170-015-7724-8
36. Ghosh T, Paul S, Paul S (2018) Modeling and experimental verification of chip flow deviation in oblique cutting. Mach Sci Technol 22(1):99–119. https://doi.org/10.1080/10910344.2017.1336630
37. Moufki A, Devillez A, Dudzinski D, Molinari A (2004) Thermomechanical modelling of oblique cutting and experimental validation. Int J Mach Tools Manuf 44(9):971–989. https://doi.org/10.1016/j.ijmachtools.2004.01.018
38. Wojciechowski S (2018) Methods of minimum uncut chip thickness estimation during cutting with defined geometry tools. Mechanik 91(8–9):664–666. https://doi.org/10.17814/mechanik.2018.8-9.104
39. Stabler G (1964) The chip flow law and its consequences. Adv Machine Tool Des Res 5:243–251
40. Mikolajczyk T, Latos H, Paczkowski T, Pimenov DY, Szynka T (2018) Innovative tools for oblique cutting. Procedia Manuf 22:166–171. https://doi.org/10.1016/j.promfg.2018.03.026
41. Mikolajczyk T, Latos H, Paczkowski T, Pimenov DY, Szynka T (2018) Using CAD CAM system for manufacturing of innovative cutting tool. 22:160–165. https://doi.org/10.1016/j.promfg.2018.03.025
42. Filippov A (2015) Cut-layer cross section in oblique turning by a single-edge tool with a curved rear surface. Russ Eng Res 35(5):385–388. https://doi.org/10.3103/S1068798X15050135
43. Grzesik W, Żak K (2011) Investigations of surface textures produced by oblique machining of different workpiece materials. Arch Mater Sci Eng 52(1):46–53
44. Aydın M, Köklü U (2017) Identification and modeling of cutting forces in ball-end milling based on two different finite element models with arbitrary Lagrangian Eulerian technique. Int J Adv Manuf Technol 92(1):1465–1480. https://doi.org/10.1007/s00170-017-0229-x
45. Aydın M, Köklü U (2020) Analysis of flat-end milling forces considering chip formation process in high-speed cutting of Ti6Al4V titanium alloy. Simul Model Pract Theory 100:102039. https://doi.org/10.1016/j.simpat.2019.102039
46. Baburaj M, Ghosh A, Shunmugam M (2017) Study of micro ball end mill geometry and measurement of cutting edge radius. Precis Eng 48:9–17. https://doi.org/10.1016/j.precisioneng.2016.10.008
47. Latos H (1978) The use of blades with rectilinear edges for processing shaped surfaces. Mechanika 59 https://kpbc.umk.pl/dlibra/publication/49162/edition/74833/content?ref=struct
48. https://mathworld.wolfram.com/Ellipse.html. Accessed June 2021
49. Todd RH, Allen DK, Alting L (1994) Manufacturing processes reference guide. Industrial Press Inc. Available from: https://books.google.co.uk/books?id=6x1smAf_PAcC&printsec=frontcover#v=onepage&q&f=false
50. Panda A, Duplak J, Michal Hatala M, Krenicky T, Peter V (2016) Research on the durability of selected cutting materials in the process of turning carbon steel MM. Science Journal:1086–1089. https://doi.org/10.17973/Mmsj.2016_10_201660
51. Matuszewski M, Mikolajczyk T, Pimenov DY, Styp-Rekowski M (2017) Influence of structure isotropy of machined surface on the wear process. Int J Adv Manuf Technol 88(9):2477–2483. https://doi.org/10.1007/s00170-016-8963-z